J Solid State Electrochem (2012) 16:3215–3226
DOI 10.1007/s10008-012-1679-6

ORIGINAL PAPER

High temperature all solid state supercapacitor based on multi-walled carbon nanotubes and poly[2,5 benzimidazole]

R. S. Hastak · P. Sivaraman · D. D. Potphode · K. Shashidhara · A. B. Samui

Received: 10 January 2012 / Revised: 31 January 2012 / Accepted: 3 February 2012 / Published online: 11 May 2012

Abstract Supercapacitor containing multi-walled carbon nanotubes (MWCNT) as the electrode material and phosphoric acid-doped poly[2,5 benzimidazole] (ABPBI) as the solid electrolyte and separator membrane has been investigated in a wide temperature range. Supercapacitors with different solid electrolyte concentrations have been fabricated and evaluated for their electrochemical performance. Specific capacitance of supercapacitors at room temperature was found to increase after the first heating cycle. Supercapacitor containing 10 wt.% of solid electrolyte in the electrode shows higher specific capacitance than the supercapacitor with liquid electrolyte. Cyclic voltammetry analysis of supercapacitors indicates high rate capability. The linear increase in the specific capacitance with temperature implies that capacitance is predominantly due to electric double layer. Electrochemical impedance analysis indicates that the mass capacitance and Warburg parameter increase with temperature, while solution resistance and leakage resistance decrease with temperature. The complex capacitance of the supercapacitors shows that both real and loss capacitances increase with temperature. The phase angle of supercapacitors is found to be around 85.2±1° at room temperature and it decreases with temperature. Galvanostatic charge–discharge cycling exhibits almost constant specific capacitance of 28 $F g^{-1}$ at room temperature. However, it increases sharply and then attains stable value of 52 $F g^{-1}$ during cycling at 100 °C. The increase in specific capacitance has been attributed to increase in surface area of the carbon nanotube (CNT), due to activation by phosphoric acid and diffusion of free phosphoric acid into the central canal of MWCNT.

Keywords Supercapacitor · Multi-walled carbon nanotubes · Solid polymer electrolyte · High temperature performance · ABPBI · Specific capacitance

R. S. Hastak · P. Sivaraman · D. D. Potphode · K. Shashidhara · A. B. Samui (✉)
Naval Materials Research Laboratory (DRDO),
Shil-Badlapur Road, Anand Nagar PO, Thane Dist,
Ambernath, Maharashtra 421 506, India
e-mail: absamui@gmail.com

A. B. Samui
e-mail: asit_samui@yahoo.com

Introduction

Supercapacitor is an electrochemical energy storage device which has higher energy density than the conventional capacitors and higher power density than the batteries [1, 2]. Based on the electrode material, supercapacitor can be classified into electric double layer capacitors and pseudocapacitors [3, 4]. In an electric double layer capacitor, an electric double layer is formed at the electrode/electrolyte interface, and the energy storage is of electrostatic in nature. Activated carbon (AC), carbon nanotubes (CNT)s and carbon aerogels are some of the commonly used materials for electric double layer capacitors [5.6]. In pseudocapacitors, a fast reversible faradaic reaction takes place at the electrode/electrolyte interface. The charge transferred in this reaction is voltage-dependant and results in pseudocapacitance ($C = dQ/dV$) [7, 8]. Conducting polymers and metal oxides are commonly used pseudocapacitance materials.

Supercapacitors with high power density and energy density that can withstand a wide temperature range are essential for use in harsh environment like military and space applications. For such applications, solid electrolytes are preferred over liquid ones, as they can be easily handled without spillage of hazardous liquid, cause low internal corrosion, have flexibility in packaging, etc. [9–13]. Super-

capacitors containing CNTs have high power density and long cycle life [14–17]. CNTs have unique properties such as excellent conductivity, remarkable chemical resistance, high surface area and good flexibility [18–20]. Reports on high temperature performance of supercapacitor are scantly. Masarapu et al. studied the effect of temperature on the electrochemical performance of the supercapacitors containing single-walled carbon nanotube (SWCNT) and a liquid electrolyte [21]. Interface properties of electrode/electrolyte such as electric double layer formation, charge transfer, mobility of ions, etc. in solid electrolyte is different from that of liquid electrolyte [22, 23]. Hence, it is very important to have a basic understanding of the various parameters that govern the electrochemical performance of a supercapacitor at high temperature with a solid electrolyte. Performance and stability of the solid polymer electrolyte at elevated temperature need to be available for selection of solid electrolyte for supercapacitor application. Poly[2,5 benzimidazole] is well known as a high temperature stable polymer. Phosphoric acid-doped poly[2,5 benzimidazole] (ABPBI) has been investigated in proton exchange membrane fuel cells (PEMFC) and supercapacitors [24–26]. To the best of our knowledge, there is no report on the effect of temperature on supercapacitor performance having multi-walled carbon nanotubes (MWCNT) as the electrode material and ABPBI as the solid electrolyte.

In an earlier report, we have studied the performance of AC-based supercapacitor containing ABPBI [23]. In the present study, we have investigated the effect of temperature on the electrochemical performance of supercapacitor-containing MWCNT as the electrode material and ABPBI as both separator membrane and solid electrolyte. Supercapacitors containing different concentrations of MWCNT and ABPBI have been fabricated and studied over a wide temperature range from 27 to 100 °C. Supercapacitors have been characterized by cyclic voltammetry and impedance spectroscopy. Stability of supercapacitor has also been studied by galvanostatic cycling at 27° and 100 °C alternatively.

Experimental

Materials

MWCNTs were procured from Nanocyl, Belgium (grade 3100) having purity above 95%. Carbon paper was procured from Toray, Japan. Teflon suspension was supplied by Hindustan Fluorocarbon, Ltd., India. 3,4-Diaminobenzoic acid and methane sulfonic acid were procured from Sigma-Aldrich. Phosphorus pentoxide and orthophosphoric acid were purchased from Merck, India. All chemicals were used without further purification.

Synthesis of ABPBI

Synthesis of ABPBI and the membrane preparation is given elsewhere [25–27].

Preparation of electrodes

The electrode preparation with ABPBI/MWCNT, unit cell preparation, characterization and evaluation are given in Indian patent [28]. MWCNT, polytetrafluoroethylene (PTFE) and ABPBI solution (6% solution in methane sulfonic acid) were thoroughly mixed to yield a paste. The paste was then applied uniformly on carbon paper and dried at 150 °C for 24 h. The electrode composition was varied by changing the amount of ABPBI in the electrode (Table 1). The amount of MWCNT was calculated to be around 3.2 mg cm^{-2}.

Preparation of unit cell

Unit cells of size 2.5 cm×2.5 cm were prepared by placing ABPBI membrane in between two electrodes and hot pressing whole assembly at 100 °C under 10 MPa pressure for 15 min. Unit cells were then soaked in 67% phosphoric acid for 24 h. They were then taken out of the bath, extra phosphoric acid was drained out and, finally, sealed in a plastic-coated aluminum pouch. The sealed unit cells were used for various electrochemical characterizations.

Treatment of MWCNT

MWCNT was refluxed with 67% phosphoric acid at 100 °C for 2 days. Treated MWCNT was then washed thoroughly with distilled water and dried before Brunauer-Emmett-Teller (BET) surface area analysis.

Characterization

Electrochemical characterizations were carried out using a Ecochimie Autolab PGSTAT30. Electrochemical impedance spectroscopy (EIS) was carried out between the frequency range of 1 MHz and 10 mHz at 0.5 V cell potential. Transmission electron microscopy (TEM) was carried out using Philips CM 200, operated at 200 kV. BET surface area of

Table 1 Electrode composition of the supercapacitors

Electrode composition (weight ratio)	ABPBI-0	ABPBI-5	ABPBI-10	ABPBI-20
MWCNT	1	1	1	1
PTFE	0.05	0.05	0.05	0.05
ABPBI	0	0.05	0.10	0.20

phosphoric acid-treated AC was recorded by using a Thermo Fisher Scientific (Sorptomatic, 1990).

Results and discussion

In the present study, the effect of incorporation of ABPBI as the electrolyte and separator in supercapacitor, containing MWCNT as the active electrode materials, has been studied at different temperatures. ABPBI has good thermal stability and high proton conductivity even at elevated temperatures and, hence, it has been selected as the solid electrolyte. ABPBI used in this study is doped with 67% phosphoric acid. Ionic conductivity of the phosphoric acid-doped ABPBI at room temperature is about 4.7 mS cm^{-1} and found to increase linearly with temperature [23].

Cyclic voltammetry (CV) of the supercapacitors

Supercapacitors with different concentrations of ABPBI in the electrode were scanned at different rates in the voltage range of 0–1 V. Figure 1 shows the specific capacitance of the supercapacitors with different concentrations of ABPBI, calculated from the cyclic voltammetry (CV) at 0.5 V at room temperature using Eq. 1:

$$C = \frac{I_a + I_c}{2ms} \quad (1)$$

where I_a and I_c are the anodic and cathodic currents at 0.5 V, m is the mass of MWCNT in the unit cell and s is scan rate of the CV [29]. The specific capacitance of ABPBI-0 is found to be higher than other supercapacitors. ABPBI-5 is found to have the lowest specific capacitance throughout the entire scan range studied. However, ABPBI-10 and ABPBI-20 show higher specific capacitance than ABPBI-5. The decrease in specific capacitance with increase in scan rate, especially at higher rates, is found to be higher for ABPBI-0 than other supercapacitors. ABPBI-0 contains liquid

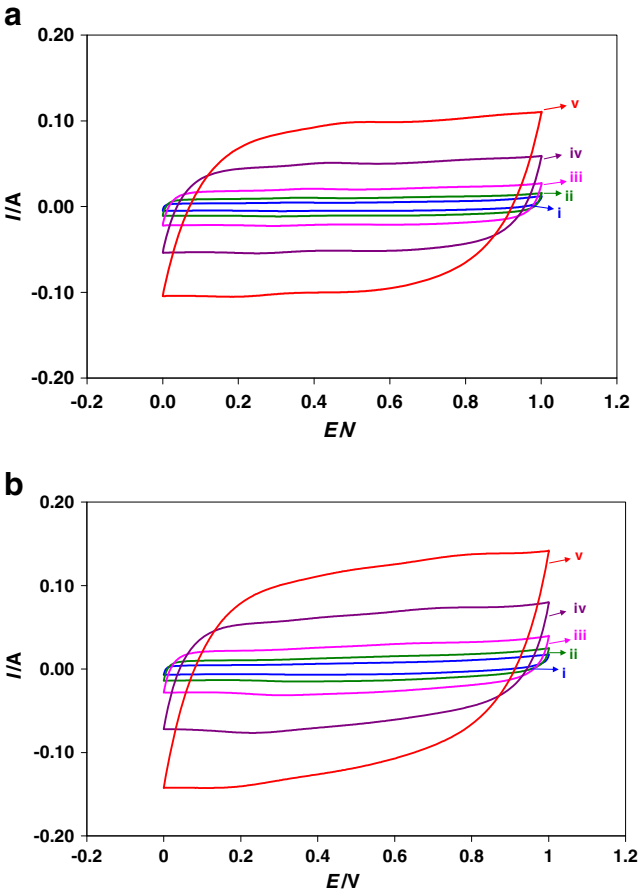

Fig. 2 CV of supercapacitor ABPBI-10 at different scan rates at room temperature. **a** Before first heating cycle. **b** After first heating cycle. *i* 25, *ii* 50, *iii* 100, *iv* 250 and *v* 500 mV s^{-1}

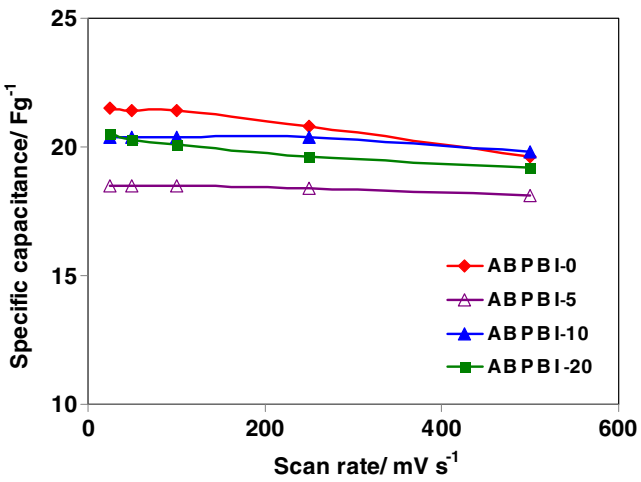

Fig. 1 Specific capacitance of supercapacitors as a function of scan rate

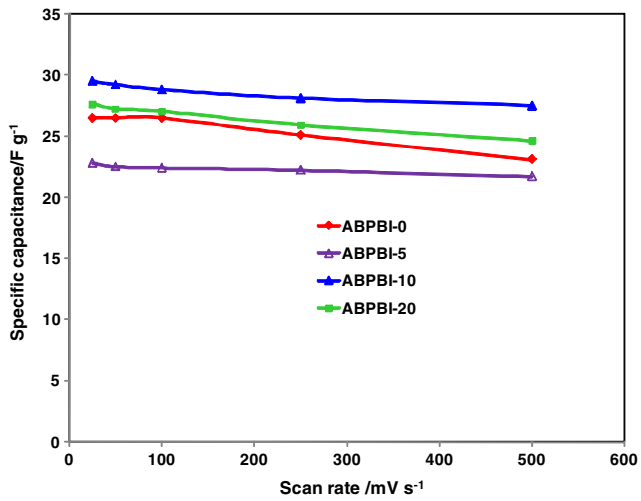

Fig. 3 Specific capacitance of supercapacitors at different scan rates after the first heating cycle

electrolyte and, hence, show higher specific capacitance at lower scan rates. However, at high scan rates, the extent of electric double layer formation in compliance with the increase in the scan rate may be less due to delay in the diffusion of ions to the vicinity of the electric double layer. In supercapacitors containing solid electrolyte, due to intimate mixing of solid electrolyte and MWCNT, the diffusion length of ions is expected to be shorter [9]. Hence, the decrease in specific capacitance with increase in scan rate is observed to be less for supercapacitors containing solid electrolyte (ABPBI-5 to ABPBI-20) than that of phosphoric acid (ABPBI-0).

CV measurements of supercapacitors at elevated temperature were carried out at predetermined temperatures in the range of 27–100 °C. The CV of ABPBI-10 at room temperature at different scan rates before and after heating is given in Fig. 2a and b, respectively. After the supercapacitors were subjected to heating cycle, specific capacitance measured subsequently at room temperature increases as compared to the original value. The increase in the current values of CV at different scan rates, after the first heating cycle (Fig. 2b), clearly indicates the increase in specific capacitance of the supercapacitor. The same trend is observed for all the supercapacitors studied (Fig. 3). At room temperature, CV of supercapacitors shows rectangular profile and this implies that the capacitance is mainly due to the electric double layer formation. Even at increased scan rates, there is no appreciable change in CV profile and specific capacitance values (Fig. 3). This clearly indicates that supercapacitors have high rate capability. It is found that ABPBI-10 shows specific

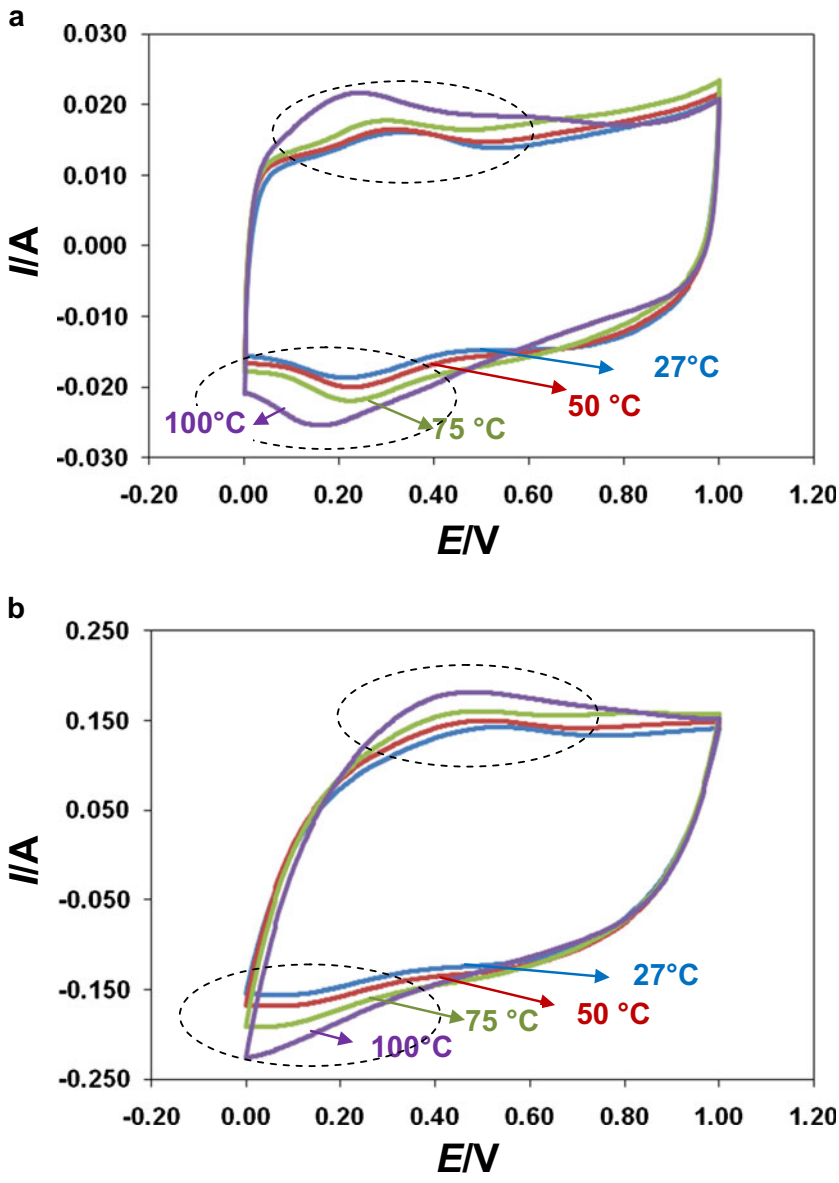

Fig. 4 CV of ABPBI-10 at different temperatures. **a** At 50 mV s^{-1} and **b** at 500 mV s^{-1}

capacitance of 29.5 F g^{-1} at a scan rate of 25 mV s^{-1}, which is highest among all supercapacitors after the first heating cycle. The increase in specific capacitance for ABPBI-10 at a scan rate of 25 mV s^{-1} is about 45% as compared to that observed before heating. However, it is only 23% for ABPBI-0. The increase in specific capacitance after the first heating cycle indicates increase in electrolyte conductivity as well as electrochemically active electrode/electrolyte interface. Ma et al. found most conductive species in phosphoric acid-doped membranes were unbound phosphoric acid [30]. Wannek et al. reported that the conductivity of ABPBI increases during the second heating cycle [31]. They related this phenomenon to the sweat out of some liquid at high temperatures, which did not re-enter the membrane during cooling, and this increased the surface conductivity of ABPBI. In the present case, also, the same effect is expected. Excess of phosphoric acid which sweat out of membrane after heating can penetrate into the MWCNT to form excess electric double layer. Solution resistance of the ABPBI-10 is also decreased from 0.867 to 0.771 Ω, after the first heating cycle due to this effect.

Figure 4a and b show the CV of ABPBI-10 carried out at different temperatures at a scan rate of 50 and 500 mV s^{-1}, respectively, during the second heating cycles. During the second heating cycle, pseudocapacitance peaks started to appear (shown as ovals in the Fig. 4). Fourier transform infrared spectroscopy (FTIR) analysis of MWCNT treated with phosphoric acid at 100 °C shows that there is no additional functional group generation on the surface (figure not shown). This indicates that the electrolyte must be physiosorbed on the surface of MWCNT. Masarapu et al. also reported a similar increase after the heating cycle for SWCNT with liquid electrolyte [21]. The

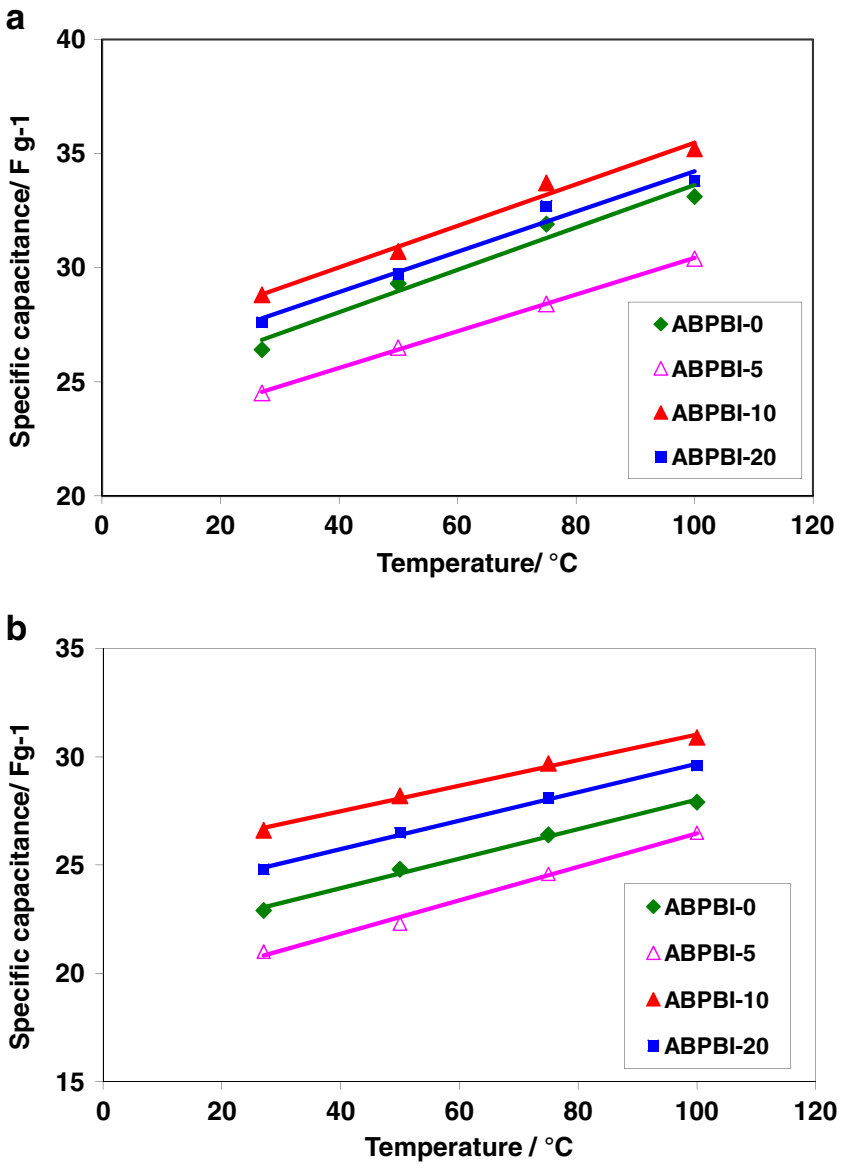

Fig. 5 Specific capacitance of supercapacitors as a function of temperature, at different scan rates. **a** 50 mV s^{-1} and **b** 500 mV s^{-1}

redox peaks associated with pseudocapacitance shift to higher voltage with increase in scan rate. Generally, when the scan rate is increased, oxidation peak shifts to higher voltage, while reduction peak shifts to lower voltage [32]. From the CV, it can be inferred that capacitance is predominantly due to double layer and pseudocapacitance also adding to overall capacitance.

Figure 5a and b show the effect of temperature on the specific capacitance of all the supercapacitors at scan rates of 50 and 500 mV s^{-1}, respectively, during the second heating cycle. All the supercapacitors show linear increase in the specific capacitance with increasing temperature. Specific capacitance of ABPBI-10 increases from 28.8 Fg^{-1} at room temperature to 35.2 Fg^{-1}. Increase in the specific capacitance can be attributed to three reasons. Firstly, due to the increase in temperature, the dissociation of ions pairs in the electrolyte increase and, hence, concentration of ions at the vicinity of electrode–electrolyte interface increase and result in enhanced double layer formation. Secondly, at high temperature, the kinetic energy of ions is high and, hence, diffusion of ions into the inner canal of MWCNT results in more amount of charge accumulation. Frackowiak et al. reported that accumulation of charges in the central canal of CNT can enhance the capacitance if the tips of the CNTs are open [18–20, 33, 34]. TEM of the MWCNT (Fig. 6) indicates the tips are mostly opened. Hence, ions will likely penetrate into the central canal of MWCNT and result in more accumulation of charges. Simon et al. had shown that the ions can even desolvate in order to enter into the pores which are of single ion size [6, 35, 36]. Thirdly, in addition to double layer capacitance, increase in temperature results in physiosorbtion of electrolyte ions on the surface of MWCNT, and resultant pseudocapacitance also contributes to the increase in specific capacitance.

It was observed that specific capacitance of ABPBI-10 is the highest among all the supercapacitor after the first heating cycle. During electrochemical measurements, the supercapacitor unit cells are kept under pressure. As ABPBI-0 contained liquid electrolyte, the chances of squeezing out of excess electrolyte from the cell could be more. During the second heating cycle, ABPBI-0 might not have enough electrolytes for the excess double layer formation at elevated temperature. On the other hand, ABPBI-10 containing solid electrolyte can hold more amount of phosphoric acid even under high pressure. However, with further increase in concentration of ABPBI, the contact between MWCNTs reduces due to more amount of coverage of solid electrode over MWCNT and, hence, the specific capacitance decreases at higher concentration. From the CV studies, it can be concluded that ABPBI-10 has optimum concentration of solid electrolyte.

Electrochemical impedance spectroscopy (EIS) of supercapacitors

EIS was carried out to understand the temperature dependence of capacitive and resistive components of the supercapacitor

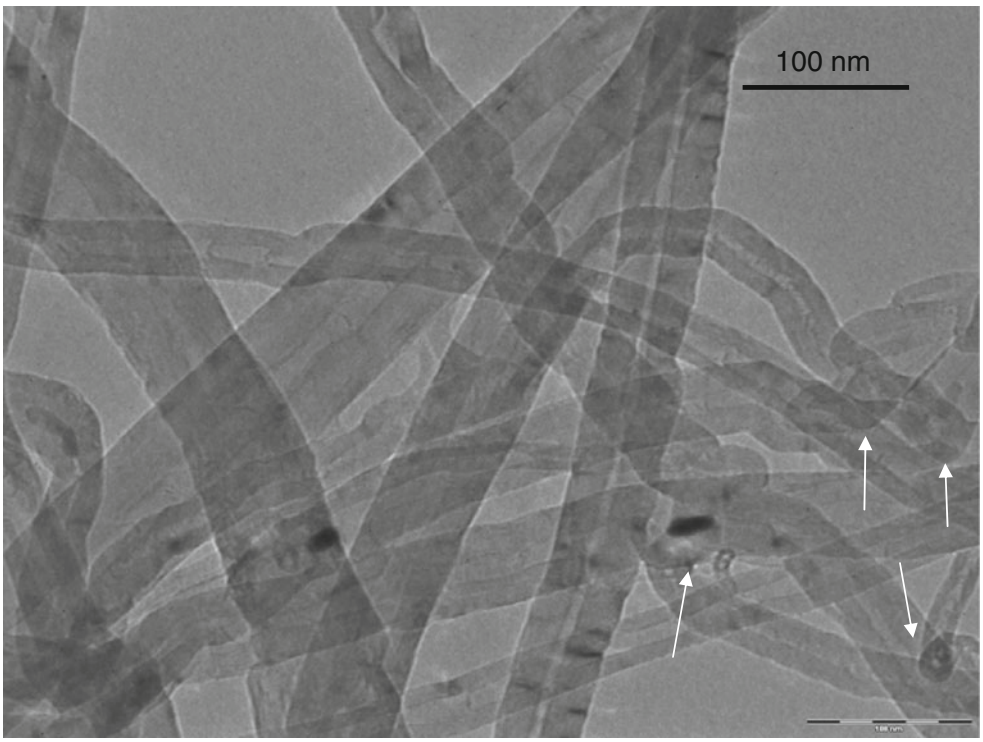

Fig. 6 TEM of MWCNT. The *arrows* indicate the opening at the tips of MWCNT

[1]. EIS analysis were carried out for ABPBI-0 and ABPBI-10, as the former contains liquid electrolyte while the latter contains optimum amount of solid electrolyte in the electrode of the supercapacitor. Figure 7a and b illustrate the Nyquist spectra of ABPBI-0 and ABPBI-10 carried out at different temperatures, respectively. EIS for all the supercapacitors is carried out at a cell potential of 0.5 V in the frequency range of 10 mHz to 1 MHz.

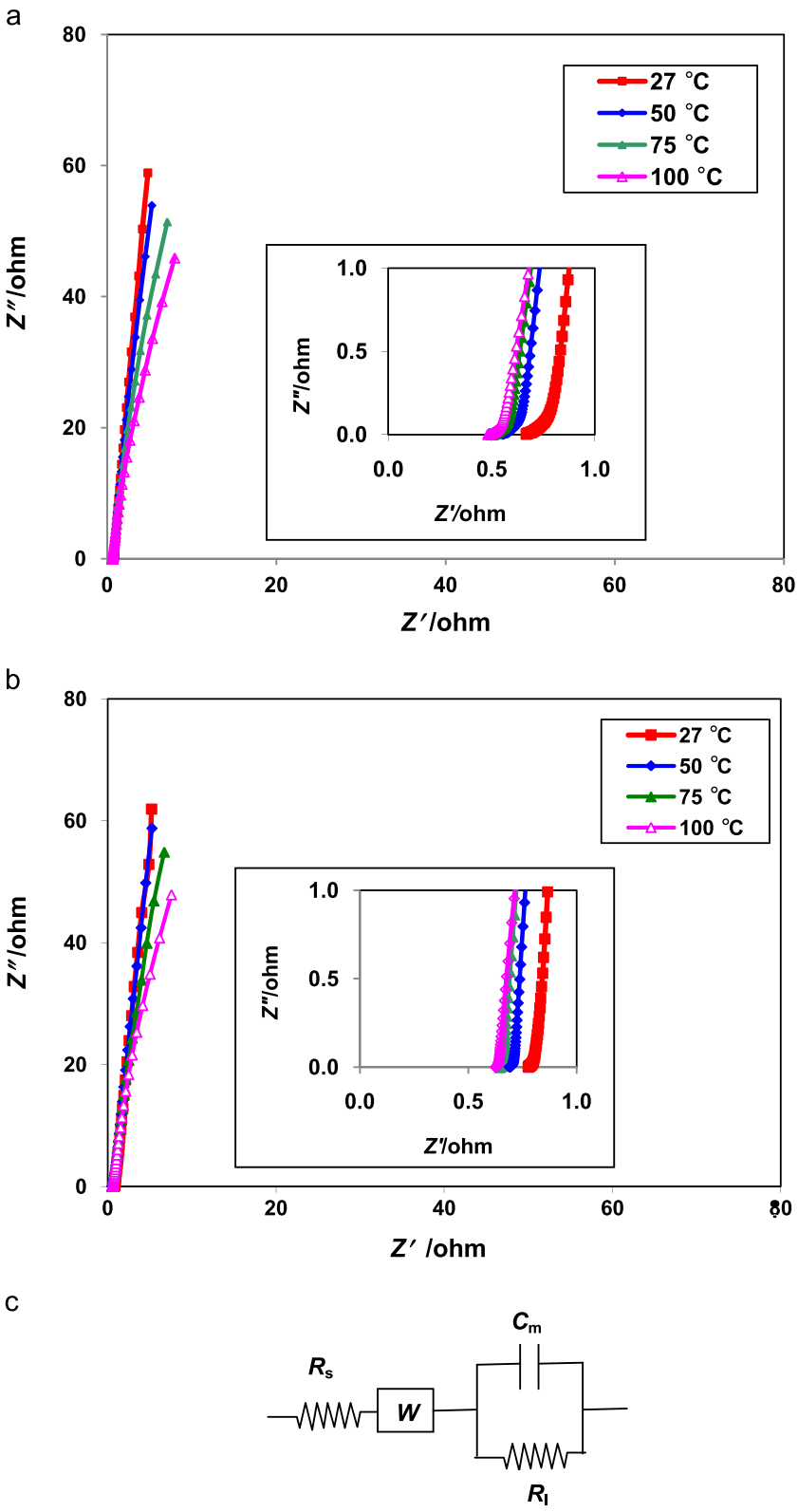

Fig. 7 Nyquist plot of supercapacitors. **a** ABPBI-0, **b** ABPBI-10 and **c** Randles equivalent circuit. R_s solution resistance, W Warburg parameter, R_l leakage resistance, C_m mass capacitance

From the Nyquist plot, solution resistance of the electrolyte (R_s) can be determined from the Z' axis intercept at the high frequency end. On decreasing the frequency, spectrum generally shows a semicircle which is represented by a parallel combination of interfacial capacitance (C_i) and resistance (R_i). However, this semicircle shifts the capacitive behavior along the real axis and the internal resistance of the cell then increases to the $R_s + R_i$ value. In the present case, absence of the semicircle indicates good contact between the current collector and the electrode material (inserts in Fig. 7) [37] and low internal resistance of the supercapacitor. Such behavior is observed when the pore size and length are uniform [1, 3]. At the midfrequency range, the spectrum shows the Warburg parameter (W), and this is followed by a vertical spike parallel to the Z'' axis at a low frequency range which is represented as mass capacitance C_m. Any inclination towards to Z' indicates that the capacitance (C_m) is with a leakage resistance (R_l) in parallel.

The impedance spectra of the supercapacitor can be represented by the Randles equivalent circuit and is shown in Fig. 7c. The values of capacitive and resistive components of the circuit for ABPBI-0 and ABPBI-10 at different temperatures are given in the Tables 2 and 3, respectively. As expected, R_s value decreases with increase in temperature, since the conductivity of the electrolyte increases with temperature [23]. However, R_s of ABPBI-10 is found to be slightly higher than ABPBI-0. In ABPBI-10, the solid electrolyte present in the electrode also adds to the thickness of the separator and, in turn, increases the R_s value.

It is observed that both W and C_m of the supercapacitors increase with temperature, while R_l decreases with temperature. Eq. 2 gives the relation between the Warburg parameter and temperature [38, 39]:

$$W = \frac{RT}{n^2F^2Ac\sqrt{D_c}} \tag{2}$$

where R is the gas constant, T is the absolute temperature, n is the number of the electron transferred, F is the faraday constant, A is the geometric electrode area, c is the ionic concentration and D_c is the diffusivity of ions in the electrode. From Eq. 2, it can be inferred that diffusivity and temperature are the two dominating factors which affect the Warburg parameter. The conducting mechanism of protons in ABPBI is based on proton jumping between a complex network of imidazole rings, water molecules and phosphoric acid molecules [30]. Mobility of phosphate counter ions is more than two orders of magnitude lower than that of the proton [27]. At elevated temperature, the kinetic energy of the ions increases which, in turn, increases the diffusivity of the ions in the electrode. At high temperatures, dehydration of solid electrolyte also takes place, which might decrease the diffusivity of ions [27]. Due to prolonged heating, unbound phosphoric acid might form oligophosphoric acid and the migration of higher molecular weight species might be difficult [40, 41]. However, the net increase in diffusivity to overcome temperature effect in Eq. 2 might be less and, hence, Warburg parameter increases with temperature. The higher Warburg parameter of ABPBI-10 is due to the obvious reason that at a given temperature, diffusivity of ions in the solid electrolyte is less compared to liquid electrolyte. Mass capacitance calculated from the fitting values is found to be close to that determined by CVs.

Table 2 Equivalent circuit fitting parameters for ABPBI-0 at different temperatures

Fitting parameters	R_s (Ω)	W (Ω $s^{-1/2}$)	R_l (kΩ)	C_m (F g^{-1})
27 °C	0.652	1.25	1.602	26.5
50 °C	0.566	1.78	0.769	27.9
75 °C	0.516	1.9	0.476	30.4
100 °C	0.497	2.02	0.326	32.5

Table 3 Equivalent circuit fitting parameters for ABPBI-10 at different temperatures

Fitting parameters	R_s (Ω)	W (Ω $s^{-1/2}$)	R_l (kΩ)	C_m (F g^{-1})
27 °C	0.771	3.23	0.776	28.5
50 °C	0.689	3.64	0.552	30.9
75 °C	0.644	3.85	0.360	32.4
100 °C	0.624	3.61	0.252	35.5

Leakage resistance, R_l, is found to decrease with increase in temperature. Leakage resistance is due to the parasitic reactions in the supercapacitor. At elevated temperature, the rate of parasitic reactions might be quite high and, hence, leakage resistance decreases [42]. Compared to liquid electrolyte, the loss in solid electrolyte is found to be more.

The complex form of frequency-dependant impedance is defined by:

$$Z(\omega) = Z'(\omega) + iZ''(\omega) \tag{3}$$

where Z' represents the real part of impedance and Z'' represents the imaginary part of the impedance. Similarly, the complex form of frequency-dependant capacitance can be defined as:

$$C(\omega) = C'(\omega) - iC''(\omega) \tag{4}$$

where

$$C' = \frac{-Z''(\omega)}{\omega|Z(\omega)|^2}. \tag{5}$$

$$C'' = \frac{Z'(\omega)}{\omega|Z(\omega)|^2}. \tag{6}$$

C' represents the real part of the frequency-dependant capacitance, while C'' represents the imaginary part of the frequency-dependant capacitance [43, 44]. C' corresponds to the capacitance measure by galvanostatic charge–discharge or CV methods. C'' represents the loss capacitance, in other words, energy loss due by irreversible process that leads to hysteresis. This could be dielectric loss of the medium [43]. Figures 8 and 9 illustrate the C' and C'' for ABPBI-0 and ABPBI-10 as a function of frequency, respectively. From Fig. 8, it is evident that the specific capacitance increases with temperature and was found to be close to the values obtained by CV. The loss capacitance also increases with increase in temperature. The loss capacitance of ABPBI-10 is found to be slightly higher compared to ABPBI-0. The dielectric loss of a solid will be comparatively higher than liquid, since dipole orientation in compliance to the applied AC signal in solid will be more difficult than in liquid.

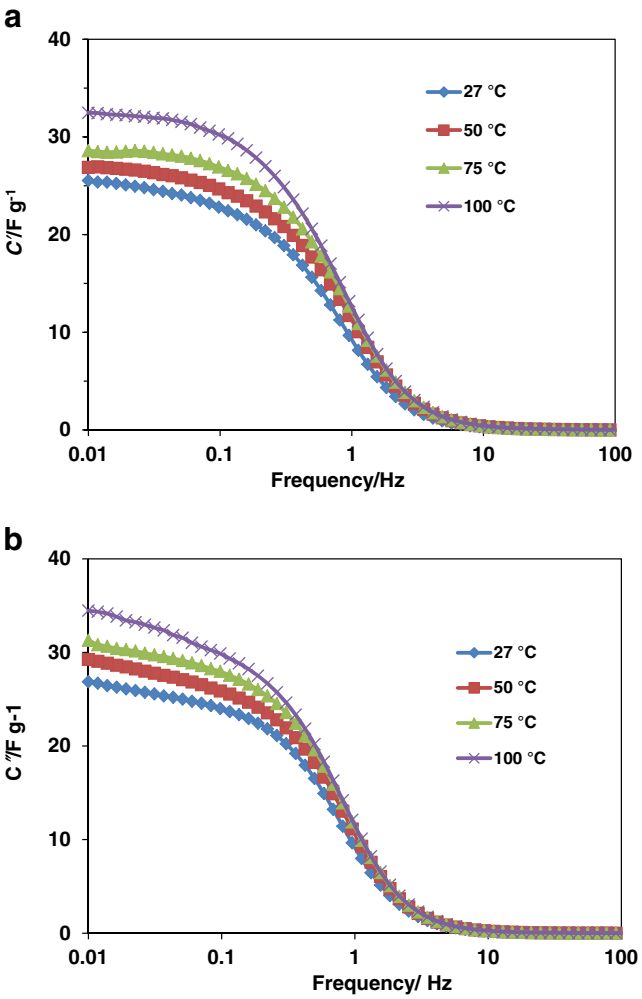

Fig. 8 Real capacitance supercapacitors at different temperatures, **a** ABPBI-0 and **b** ABPBI-10

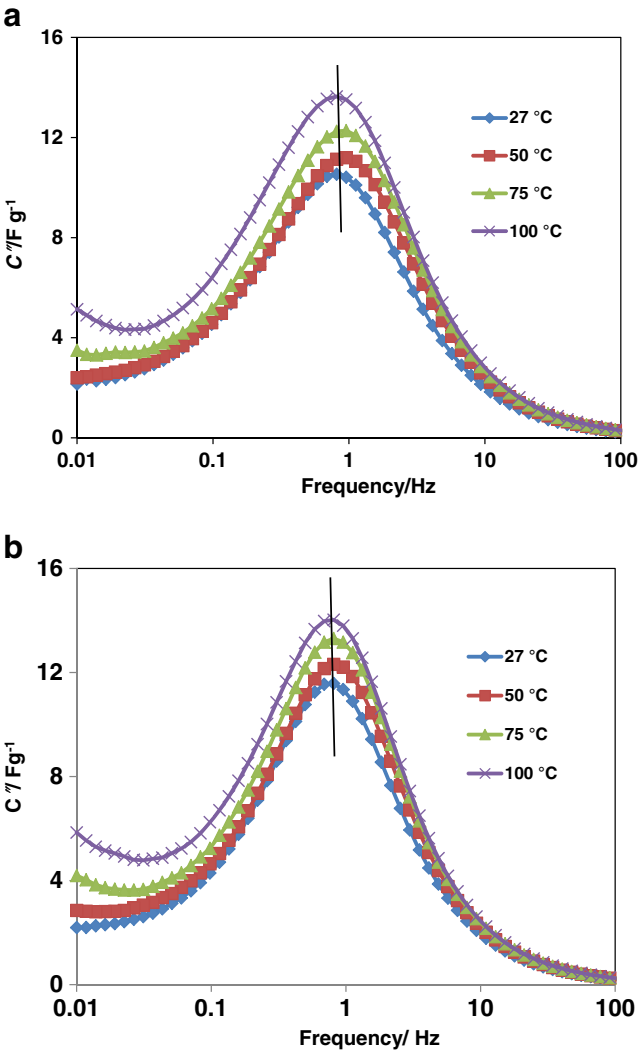

Fig. 9 Loss capacitance supercapacitors at different temperatures, **a** ABPBI-0 and **b** ABPBI-10

The peak C'' in Fig. 9 corresponds to a frequency, f_0, and the time constant is defined by $\tau_0 = 1/f_0$. The time constant represents the dielectric relaxation time and corresponds to the figure of merit of the supercapacitor [44, 45]. It is the time below which the supercapacitor behavior is resistive and above, it is capacitive. In other words, at time constant,

Table 4 Time constant and phase angle of ABPBI-0 and ABPBI-10 at different temperatures

Temperature (°C)	ABPBI-0		ABPBI–10	
	τ_0 (s)	Phase angle (°)	τ_0 (s)	Phase angle (°)
27	1.23	85.2	1.23	85.3
50	1.05	84.9	1.23	84.5
75	1.05	83.4	1.23	83.1
100	1.23	82.1	1.23	81.6

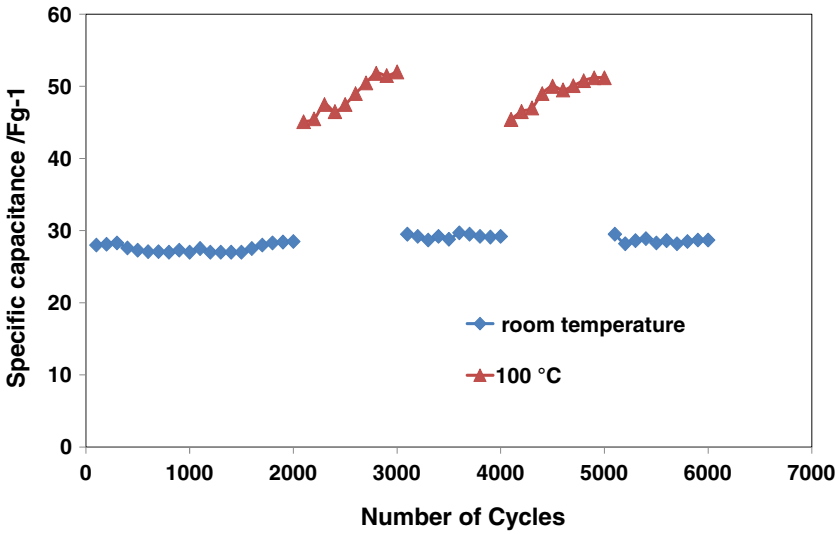

Fig. 10 Specific capacitance of ABPBI-10 as a function of galvanostatic charge–discharge cycles

τ_0, phase angle is 45°. From Table 4, it can be observed that the time constant of both the supercapacitors are almost constant with change in temperature. It denotes the time taken for diffusion of ions on the surface of MWCNT. Marasapu et al. also indicated that the diffusion of ions takes place along the surface of SWCNT and showed that the charging process is temperature independent [21].

Phase angle of a capacitance is a measure of capacitance behavior. Phase angle of the supercapacitors is found to be around 85.2±0.1° at room temperature which is close to the ideal capacitor (90°). This result implies that supercapacitors have excellent capacitor behavior at room temperature. However, phase angle is found to decrease for both the supercapacitors with increase in temperature. This decrease in phase angle is due to the decrease in the leakage resistance with temperature.

Galvanostatic charge–discharge cycling

ABPBI-10 has been subjected to continuous charge–discharge cycling. The specific capacitance as a function of charge–discharge cycles is shown in Fig. 10. Initial 2,000 cycles have been carried out at room temperature and, thereafter, 1,000 cycles each at 100 °C and room temperature alternatively. The charging–discharging cycles has been carried out in the voltage range of 0–0.8 V at a current rate of 1 A g^{-1}. It is observed that the room temperature-specific capacitance increases slowly from 28.2 to 29.8 F g^{-1}. However, during high temperature cycling, the specific capacitance increases sharply and then attains an almost constant value. The same trend is observed for subsequent cycling at room temperature and 100 °C. Interestingly, the high temperature capacitance increases to 52 F g^{-1} which is approximately 85% more than that observed at room temperature. During initial cycles of charge–discharge, free phosphoric acid penetration into the central canal of the CNT might be very less or very slow and, hence, capacitance increase is observed to be very less. Figure 11 shows the nitrogen adsorption isotherm of MWCNT treated with phosphoric acid at 100 °C for 0, 24 and 48 h. Surface areas are 239, 254 and 319 m^2 g^{-1} for 0-, 24- and 48-h treated MWCNT, respectively. Phosphoric acid is a good oxidizing agent for carbonaceous materials [5, 46, 47]. Treatment of carbon with phosphoric acid, at elevated temperature, generally creates a porous carbon structure [23, 48]. In the present case, also, phosphoric acid may activate the surface of MWCNT at elevated temperature of 100 °C. This may increase the micropores of the MWCNT and might also open pores that lead to the central canal. Hence, at elevated temperature, the capacitance increases sharply due to migration of free acid into the central canal of MWCNT. Jurwicz

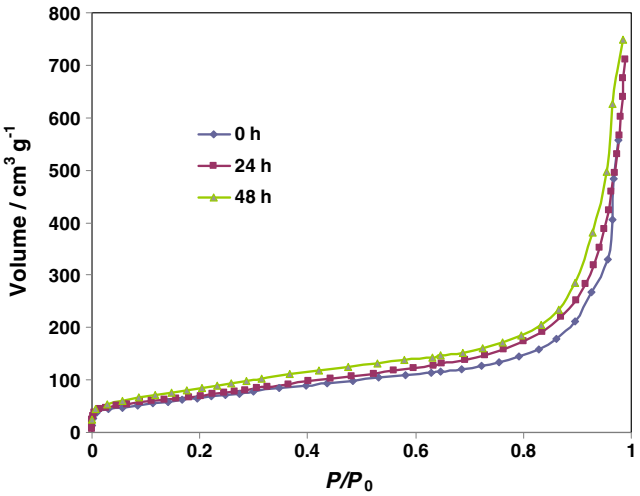

Fig. 11 Nitrogen adsorption isotherm of MWCNT treated with 67% phosphoric acid at 100 °C

et al. also reported that KOH treatment of (CNT)s increased their surface area. The surface area increase attributed to the opening of tips of (CNT)s and creation of micropores along the walls [33].

Conclusion

MWCNT supercapacitor containing different concentrations of ABPBI was fabricated, and their electrochemical performance was studied over a temperature range of 27–100 °C. The specific capacitance of supercapacitors at room temperature increased after the first heating cycle. ABPBI-10 showed a specific capacitance of 28.8 Fg^{-1} at 50 mV s^{-1} scan rate at room temperature, which was the highest among all the supercapacitors studied. Rectangular CV profile of supercapacitor indicated good capacitor behavior even at high scan rates. Specific capacitance was found to increase linearly with temperature and indicated that the capacitance was largely due to electric double layer, even though some pseudocapacitance behavior was noticed. EIS of supercapacitors analyzed with Randles equivalent circuit. Complex capacitance was resolved into real and loss capacitances and was found that both the capacitances increased with temperature. The time constant, τ_0, was found to be independent of temperature. Phase angle of supercapacitor was about 85.2± 1° at room temperature and it decreased with temperature. Galvanostatic charge–discharge cycles were carried out for ABPBI-10. Specific capacitance of supercapacitor was stable during room temperature cycling; however, at 100 °C, the specific capacitance initially increases and attains a stable value. The specific capacitance at 100 °C was found to be 52 Fg^{-1} which was 85% more than that at room temperature. The increase in specific capacitance is attributed to increase in surface area due to activation by phosphoric acid resulting in diffusion of ion into the central canal of MWCNT.

References

1. Conway BE (1999) Electrochemical supercapacitors, scientific fundamentals and technological applications. Kluwer/Plenum, New York
2. Burke A (2000) Ultracapacitors: why, how, and where is the technology. J Power Sourc 91:37–50
3. Kotz K, Carlen M (2000) Principles and applications of electrochemical capacitors. Electrochim Acta 45:2483–2498
4. Sarangapani S, Tilak BV, Chen CP (1996) Materials for electrochemical capacitors, theoretical and experimental constraints. J Electrochem Soc 143:3791–3799
5. Pandolfo AG, Hollenkamp AF (2006) Carbon properties and their role in supercapacitors. J Power Sourc 157:11–27
6. Simon P, Gogotsi Y (2008) Materials for electrochemical capacitors. Nat Mater 7:845–854
7. Rudge A, Davey J, Raistrick I, Gottesfeld S, Ferraris JP (1994) Conducting polymers as active materials in electrochemical capacitors. J Power Sourc 47:89–107
8. Rudge A, Raistrick I, Gottesfeld S, Ferraris JP (1994) A study of the electrochemical properties of conducting polymers for application in electrochemical capacitors. Electrochim Acta 39:273–287
9. Lufrano F, Staiti P (2004) Performance improvement of Nafion based solid state electrochemical supercapacitor. Electrochim Acta 49:2683–2689
10. Sivaraman P, Hande VR, Mishra VS, Rao CS, Samui AB (2003) All-solid supercapacitor based on polyaniline and sulfonated poly (ether ether ketone). J Power Sourc 124:351–354
11. Sivaraman P, Rath SK, Hande VR, Thakur AP, Patri M, Samui AB (2006) All-solid-supercapacitor based on polyaniline and sulfonated polymers. Synth Met 156:1057–1064
12. Sivaraman P, Kushwaha RK, Shashidhara K, Hande VR, Thakur AP, Samui AB, Khandpekar MM (2010) All solid supercapacitor based on polyaniline and crosslinked sulfonated poly[ether ether ketone]. Electrochim Acta 55:2451–2456
13. Ishikawa M, Morita M, Ihara M, Matsuda Y (1994) Electric double layer capacitor composed of activated carbon fiber cloth electrodes and solid polymer electrolytes containing alkyl ammonium salts. J Electrochem Soc 141:730–1734
14. Najafabadi AI, Yamada T, Futaba DN, Yudasaka M, Takagi H, Hatori H, Iijima S, Hata K (2011) High-power supercapacitor electrodes from single-walled carbon nanohorn/nanotube composite. ACS Nano 5:811–819
15. Futaba DN, Hata K, Yamada T, Hiraoka T, Hayamizu Y, Kakudate Y, Tanaike O, Hatori H, Yumur M, Iijuma S (2006) Shape-engineerable and highly densely packed single-walled carbon nanotubes and their application as super-capacitor electrodes. Nat Mater 5:987–994
16. Lee SW, Kim BS, Chne S, Horn YS, Hammond PT (2009) Layer-by-layer assembly of all carbon nanotube ultrathin films for electrochemical applications. J Am Chem Soc 131:671–679
17. Pint CL, Nicholas NW, Xu S, Sun Z, Tour JM, Schmidt HK, Gordon RG, Hauge RH (2011) Three dimensional solid-state supercapacitors from aligned single-walled carbon nanotube array templates. Carbon 49:4890–4897
18. Frackowiak E, Metenier K, Bertagna V, Beguin F (2000) Supercapacitor electrodes from multiwalled carbon nanotubes. Appl Phys Lett 77:2421–2423
19. Frackowiak E, Beguin F (2002) Electrochemical storage of energy in carbon nanotubes and nanostructured carbons. Carbon 40:1775–1787
20. Frackowiak E, Jurewicz K, Delpeux S, Beguin F (2001) Nanotubular materials for supercapacitors. J Power Sourc 97–98:822–825
21. Masarapu C, Zeng HF, Hung KH, Wei B (2009) Effect of temperature on capacitance of carbon nanotube supercapacitors. ACS Nano 8:2199–2206
22. Hung K, Masarapu C, Ko T, Wei B (2009) Wide-temperature range operation supercapacitors from nanostructured activated carbon fabric. J Power Sourc 193:944–949
23. Hastak RS, Sivaraman P, Potphode DD, Shashidhara K, Samui AB (2012) All solid supercapacitor based on activated carbon and poly [2,5-benzimidazole] for high temperature application. Electrochim Acta 59:296–303
24. Kim HJ, An SJ, Moon JY, Cho SY, Eun YC, Yoon HK, Park Y, Kweon HJ, Shin EM (2005) Macromol Rapid Comm 25:1410–1413
25. Asensio A, Ramero PS (2005) Recent developments on proton conducting poly [2, 5 benzimidazole] (ABPBI) membranes for high temperature polymer electrolyte membrane fuel cells. Fuel Cell 5:336–343
26. Romero PG, Chojak M, Gallegos KC, Sensio JA, Kulesza PJ, Pastor NC, Cantu ML (2003) Hybrid organic–inorganic nano-

composite materials for application in solid state electrochemical supercapacitors. Electrochem Comm 5:149–153
27. Li Q, Jensen JO, Savinell RF, Bjerrum NJ (2009) High temperature proton exchange membranes based on polybenzimidazole for fuel cells. Prog Polym Sci 34:447–449
28. Hastak RS, Sivaraman P, Potphode DD, Shashidhara K, Samui AB (2012) Solid polymer electrolyte and carbon nanotubes containing supercapacitor for high temperature application. Indian Patent (Provisional) submitted
29. Snook GA, Kao P, Best AS (2011) Conducting-polymer-based supercapacitor devices and electrodes. J Power Sourc 196:1–12
30. Ma YL, Wainright JS, Litt MH, Savinell RF (2004) Conductivity of PBI membranes for high temperature polymer electrolyte fuel cells. J Electrochem Soc 151:A8–A16
31. Wannek C, Lehnert W, Mergel J (2009) Membrane electrode assemblies for high-temperature polymer electrolyte fuel cells based on poly(2,5-benzimidazole) membranes with phosphoric acid impregnation via the catalyst layers. J Power Sourc 192: 258–266
32. Bard AJ, Faulkner LR (2001) Electrochemical methods: fundamentals and applications, 2nd edn. Wiley, USA
33. Jurewicz K, Babel K, Pietrzak R, Delpeux S, Wachowska H (2006) Capacitance properties of multi-walled carbon nanotubes modified by activation and ammoxidation. Carbon 44:2368–2375
34. Ye JS, Liu X, Cui HF, Zhang WD, Sheu FS, Lim TM (2005) Electrochemical oxidation of multiwalled carbon nanotubes and its application to electrochemical double layer capacitors. Electrochem Comm 7:249–255
35. Chmiola J, Yusgin G, Gogotsi Y, Portet C, Simon P, Taberna PL (2006) Anomalous increase in carbon capacitance at pore size below 1 nm. Science 313:1760–1763
36. Largeot C, Portet C, Chmiola J, Taberna PL, Gogosti Y, Simon P (2008) Relation between the ion size and pre size for an electric double-layer capacitor. J Am Chem Soc 130:2730–2731
37. Portet C, Taberna PL, Simon P, Robert CL (2004) Modification of Al current collector surface by sol–gel deposit for carbon–carbon supercapacitor applications. Electrochim Acta 49:905–912
38. Brett CMA, Brett AMO (1993) Electrochemistry—principles, methods and applications. Oxford University Press
39. Wang KP, Teng H (2007) Structural feature and double layer capacitive performance of porous carbon powder derived form polyacrylonitrile-based carbon fiber. J Electrochem Soc 154: A993–A998
40. Masson JF (2008) A brief review of the chemistry of polyphosphoric acid (PPA) and bitumen. Energy Fuel 22:2637–2640
41. Asensio JA, Borros S, Romero PG (2004) Polymer electrolyte fuel cells based on phosphoric acid-impregnated poly(2,5-benzimidazole) membranes. J Electrochem Soc 151:A304–A310
42. Conway BE, Pell WG, Liu TC (1997) Diagnostic analysis for mechanisms of self-discharge of electrochemical capacitors and batteries. J Power Sourc 65:53–59
43. Portet C, Taberna PL, Simon P, Flahaut E (2005) Influence of carbon nanotubes addition on carbon–carbon supercapacitor performance in organic electrolyte. J Power Sourc 139:371–378
44. Taberna PL, Simon P, Fauvarque JF (2003) Electrochemical characteristics and impedance spectroscopy studies of carbon-carbon supercapacitors. J Electrochem Soc 150:A 292–A 300
45. Miller J (1998) In: "Proceedings of the 8th International Seminar on Double-Layer Capacitors and Similar Energy Storage Devices" Deerfield Beach, Florida, USA, December 7–9
46. Puziy AM, Poddubnaya OI, Socha RP, Gurgul J, Wisniewski M (2008) XPS and NMR studies of phosphoric acid activated carbons. Carbon 46:2113–2123
47. Puziy AM, Poddubnaya OI, Alonso M, Garcia FS, Tascon JMD (2003) Synthetic carbons activated with phosphoric acid III. Carbons prepared in air. Carbon 41:1181–1191
48. Sobio MM, Reinoso FR, Caturla F, Selles MJ (1995) Porosity in granular carbons activated with phosphoric acid. Carbon 33:1105–1113